International Journal of Modern Engineering Research (IJMER)
www.ijmer.com Vol. 3, Issue. 5, Jul - Aug. 2013 pp-2675-2696 ISSN: 2249-6645

Effect of Radiation on Mixed Convection Flow of a Non-Newtonian Nanofluid over a Non-Linearly Stretching Sheet with Heat Source/Sink

S.Vijaya Lakshmi[1] and M. Suryanarayana Reddy[2]
[1]Research Scholar, JNTU Anantapur, Anantapuram, A.P, India.
[2]Department of mathematics, JNTUA College of engineering, Pulivendula-516 390.A.P,India

ABSTRACT: *A boundary layer analysis is presented for the effect of radiation on mixed convection flow of a non-Newtonian nanofluid in a nonlinearly stretching sheet with heat source/sink. The micropolar model is chosen for the non-Newtonian fluid since the spinning motion of the nanoparticles as they move along the streamwise direction can be best described by the micropolar fluid model. Numerical results for friction factor, surface heat transfer rate and mass transfer rate have been presented for parametric variations of the micropolar material parameters, Brownian motion parameter N_B, thermophoresis parameter N_T, radiation parameter R, heat source/sink parameter Q and Schmidt number Sc. The dependency of the friction factor, surface heat transfer rate and mass transfer rate on these parameters has been discussed.*

KEYWORDS: *Mixed Convection, Stretching Sheet, Non-Newtonian Flow, Nanofluid, Radiation, Heat source/sink.*

I. INTRODUCTION

Study of non-Newtonian fluids over a stretching surface achieved great attention due to its large number of application. In fact, the effects of non-Newtonian behavior can be determined due to its elasticity, but sometimes rheological properties of fluid are identified by their constitutive equations. In view of rheological parameters, the constitutive equations in the non-Newtonian fluids are morecomplex and thus give rise the equations which are complicated than the Navier–Stokes equations. Many of the fluids used in the oil industry and simulate reservoirs are significantly non-Newtonian. In different degree, they display shear-dependent of viscosity, thixotropy and elasticity (Pearson and Tardy [1]; Ellahi and Afza [2]; Ellahi [3]). Gorla and Kumari [4] studied the mixed convection flow of a non-newtonian nanofluid over a non-linearly stretching sheet.

Nanoparticles range in diameter between 1 and 100 nm. Nanofluids commonly contain up to a 5% volume fraction of nanoparticlesto ensure effective heat transfer enhancements. One of the main objectives of using nanofluids is to achieve the best thermal properties with the least possible (<1%) volume fraction of nanoparticles in the base fluid. The term nanofluid was first proposed by Choi [5] to indicate engineered colloids composed of nanoparticles dispersed in a base fluid. The characteristic feature of nanofluids is thermal conductivity enhancement; a phenomenon observed by Masuda et al. [6].There are many studies on the mechanism behind the enhanced heat transfer characteristics using nanofluids. Eldabe et al. [7] analyzed the effects of magnetic field and heat generation on viscous flow and heat transfer over a nonlinearly stretching surface in a nanofluid.

Micropolar fluids are subset of the micromorphic fluid theory introduced in a pioneering paper by Eringen[8]. Micropolar fluids are those fluids consisting of randomly oriented particles suspended in a viscous medium, which can undergo a rotation that can affect the hydrodynamics of the flow, making it a distinctly non-Newtonian fluid. They constitute an important branch of non-Newtonian fluid dynamics where microrotation effects as well as microinertia are exhibited. Eringen's theory has provided a good model for studying a number of complicated fluids, such as colloidal fluids, polymeric fluids and blood.

In the context of space technology and in processes involving high temperatures, the effects of radiation are of vital importance. Studies of free convection flow along a vertical cylinder or horizontal cylinder are important in the field of geothermal power generation and drilling operations where the free stream and buoyancy induced fluid velocities are of roughly the same order of magnitude. Many researchers such as Arpaci [9], Cess [10], Cheng and Ozisik [11], Raptis [12], Hossain and Takhar [13, 14] have investigated the interaction of thermal radiation and free convection for different geometries, by considering the flow to be steady. Oahimire et al.[15] studied the analytical solution to mhd micropolar fluid flow past a vertical plate in a slip-flow regime in the presence of thermal diffusion and thermal radiation. El-Arabawy [16] studied the effect of suction/injection on a micropolar fluid past a continuously moving plate in the presence of radiation. Ogulu [17] studied the oscillating plate-temperature flow of a polar fluid past a vertical porous plate in the presence of couple stresses and radiation. Rahman and Sattar [18] studied transient convective heat transfer flow of a micropolar fluid past a continuously moving vertical porous plate with time dependent suction in the presence of radiation. Mat et al. [19] studied the radiation effect on marangoni convection boundary layer flow of a nanofluid.

The heat source/sink effects in thermal convection, are significant where there may exist a high temperature differences between the surface (e.g. space craft body) and the ambient fluid. Heat Generation is also important in the context of exothermic or endothermic chemical reaction. Sparrow and Cess [20] provided one of the earliest studies using a similarity approach for stagnation point flow with heat source/sink which vary in time. Pop and Soundalgekar [21] studied unsteady free convection flow past an infinite plate with constant suction and heat source. Rahman and Sattar [22] studied magnetohydrodynamic convective flow of a micropolar fluid past a vertical porous plate in the presence of heat generation/absorption. Lin et al. [23] studied the marangoni convection flow and heat transfer in pseudoplastic non-newtonian nanofluids with radiation effects and heat generation or absorption effects.

The present work has been undertaken in order to analyze the two mixed convection boundary layer flow of a non-Newtonian nanofluid on a non-linearly stretching sheet in the presence of radiation and heat source/sink. The micropolar model is chosen for the non- Newtonian fluid since the spinning motion of the nanoparticles as they move along the streamwise direction can be best described by the micropolar fluid model. The effects of Brownian motion and thermophoresis are included for the nanofluid. The governing boundary layer equations have been transformed to a two-point boundary value problem in similarity variables and the resultant problem is solved numerically using the fourth order Runga-Kutta method along with shooting technique. The effects of various governing parameters on the fluid velocity, temperature, concentration, and Nusselt number are shown in figures and analyzed in detail.

II. MATHEMATICL ANALYSIS

Consider a steady, mixed convection boundary layer flow of a micropolar nanofluid over a non-linearly stretching sheet. The velocity components in x and y directions are u and v respectively. At the surface, the temperature T and the nano particle fraction take values T_w and C_w, respectively. The ambient values, attained as the radial distance r tends to infinity, of T and C are denoted by T_∞ and C_∞, respectively. The governing equations within boundary layer approximation may be written as:

Continuity equation

$$\frac{\partial u}{\partial x}+\frac{\partial v}{\partial y}=0 \tag{2.1}$$

Momentum equation

$$u\frac{\partial u}{\partial x}+v\frac{\partial u}{\partial y}=\left(\frac{\upsilon+\kappa}{\rho}\right)\frac{\partial^2 u}{\partial y^2}+\frac{\kappa}{\rho}\frac{\partial N}{\partial y}+g\beta_T(T-T_\infty)+g\beta_C(C-C_\infty) \tag{2.2}$$

Angular Momentum equation

$$\rho j\left(u\frac{\partial N}{\partial x}+v\frac{\partial N}{\partial y}\right)=\gamma\frac{\partial^2 N}{\partial y^2}-\kappa\left(2N+\frac{\partial u}{\partial y}\right) \tag{2.3}$$

Energy equation

$$u\frac{\partial T}{\partial x}+v\frac{\partial T}{\partial y}=\alpha_m\frac{\partial^2 T}{\partial y^2}-\frac{\alpha_m}{k}\frac{\partial q_r}{\partial y}+\tau\left(D_B\frac{\partial C}{\partial y}\frac{\partial T}{\partial y}+\left(\frac{D_T}{T_\infty}\right)\left(\frac{\partial T}{\partial y}\right)^2\right)+\frac{Q_0}{(\rho c)_f}(T-T_\infty) \tag{2.4}$$

Species equation

$$u\frac{\partial C}{\partial x}+v\frac{\partial C}{\partial y}=D_B\frac{\partial^2 C}{\partial y^2}+\frac{D_T}{T_\infty}\frac{\partial^2 T}{\partial y^2} \tag{2.5}$$

The boundary conditions may be written as:

$$u=u_w=cx^n, v=0, N=-m\frac{\partial u}{\partial y}, T=T_w, C=C_w \quad \text{at} \quad y=0 \tag{2.6}$$

$$u\to 0, N\to 0, T\to T_\infty, C\to C_\infty \quad \text{as } y\to\infty \tag{2.7}$$

In the above equations, *N* is the component of microrotation vector normal to the *xy*-plane; U_∞ the free stream velocity, D_B is the Brownian diffusion coefficient, D_T is the Thermophoretic diffusion coefficient, α_m is the thermal diffusivity, q_r is the heat flux, Q_0 is the heat generation or absorption coefficient such that $Q_0>0$ corresponds to heat generation while $Q_0<0$ corresponds to heat absorption, g is the acceleration due to gravity, ρ_f is the material density of the base fluid, ρ_p is the material density of nanoparticles, $(\rho c)_f$ and $(\rho c)_p$ are the heat capacity of the base fluid and the effective heat capacity of the nano particle material, respectively and μ,κ,ρ,j,γ and α_m are respectively the dynamic viscosity, vortex viscosity (or the microrotation viscosity), fluid density, microinertia density, spin gradient viscosity and thermal diffusivity. We follow the work of many authors by assuming that $\gamma=(\mu+\kappa/2)j=\mu(1+K/2)j$ where $K=\kappa/\mu$ is the material parameter. This assumption is invoked to allow the field of equations to predict the correct behavior in the limiting case when the microstructure effects become negligible and the total spin *N* reduces to the angular velocity (see Ahmadi14 or Yücel15).

The radiative heat flux q_r is described by Roseland approximation such that

$$q_r=-\frac{4\sigma^*}{3k'}\frac{\partial T^4}{\partial y} \tag{2.8}$$

where σ^* *and* k' are the Stefan-Boltzmann constant and the mean absorption coefficient, respectively. Following Chamkha [20], we assume that the temperature differences within the flow are sufficiently small so that they T^4 can be expressed as a linear function after using Taylor series to expand T^4 about the free stream temperature T_∞ and neglecting higher-order terms. This result is the following approximation:

$$T^4 \approx 4T_\infty^3 T - 3T_\infty^4 \tag{2.9}$$

In view of equations (2.8) and (2.9), equation (2.4) reduces to

$$u\frac{\partial T}{\partial x} + v\frac{\partial T}{\partial y} = \alpha_m\left(1+\frac{16\sigma^* T_\infty^3}{3kk'}\right)\frac{\partial^2 T}{\partial y^2} + \tau\left(D_B\frac{\partial C}{\partial y}\frac{\partial T}{\partial y}+\left(\frac{D_T}{T_\infty}\right)\left(\frac{\partial T}{\partial y}\right)\right)^2 + \frac{Q_0}{(\rho c)_f}(T-T_\infty) \tag{2.10}$$

Proceeding with the analysis, we de.ne the following transformations:

$$\psi = \sqrt{\frac{2\upsilon}{c(n+1)}}\frac{1}{x^{(n+1)/2}}cx^n f(\eta), \eta = \sqrt{\frac{c(n+1)}{2\upsilon}}x^{(n-1)/2}y$$
$$N = cx^n\sqrt{\frac{c(n+1)}{2\upsilon}}x^{(n-1)/2}g(\eta), \theta(\eta) = \frac{T-T_\infty}{T_w-T_\infty}, \phi(\eta) = \frac{C-C_\infty}{C_w-C_\infty} \tag{2.11}$$

The mass conservation equation (2.1) is satisfied by the Cauchy-Riemann Equations

$$u = \frac{\partial\psi}{\partial y} \text{ and } v = -\frac{\partial\psi}{\partial x}. \tag{2.12}$$

The Darcian velocity components:

$$u = cx^n f'(\eta), v = -\frac{\eta\upsilon}{y}\left[f(\eta)+\frac{(n-1)}{(n+1)}\eta f'(\eta)\right], \alpha_m = \frac{k_m}{(\rho c)_f}, \tau = \frac{(\rho c)_p}{(\rho c)_f}, Gr_x = \frac{g_c\beta(T_w-T_\infty)x^3}{\upsilon^2}$$
$$\mathrm{Re}_x = \frac{u_w x}{\upsilon} = \frac{cx^{n+1}}{\upsilon}, N_B = \frac{(\rho c)_p D_B(C_w-C_\infty)}{(\rho c)_f\alpha_m}, \lambda = \frac{Gr_x}{\mathrm{Re}_x^2}, N_T = \frac{(\rho c)_p D_T(T_w-T_\infty)}{(\rho c)_f\alpha_m T_\infty} \tag{2.13}$$
$$R = \frac{4\sigma^* T_\infty^3}{kk'}, Q = \frac{Q_1 x}{u_w(\rho c)_f(T_w-T_\infty)}, \mathrm{Pr} = \frac{\upsilon}{\alpha_m}, Sc = \frac{\upsilon}{D_B}, S = \frac{\beta^*(C_w-C_\infty)}{\beta(T_w-T_\infty)}$$

In view of the Equation (2.11), (2.12) and (2.13) , and the equations (2.2), (2.3), (2.5) and (2.10) reduce to the following non-dimensional form

$$(1+K)f''' + ff'' - \frac{2n}{n+1}f'^2 + Kg' + \frac{2}{n+1}\lambda(\theta+S\phi) = 0 \tag{2.14}$$

$$(1+K/2)g'' + fg' - \frac{3n-1}{n+1}f'g - \frac{2K}{n+1}(2g+f'') = 0 \tag{2.15}$$

$$\left(1+\frac{4}{3}R\right)\frac{1}{\mathrm{Pr}}\theta'' + \frac{1}{\mathrm{Pr}}N_B\theta'\phi' + \frac{1}{\mathrm{Pr}}N_T(\theta')^2 + \frac{2}{n+1}Q\theta + f\theta' = 0 \tag{2.16}$$

$$\frac{1}{Sc}\phi'' + \frac{1}{Sc}\frac{N_T}{N_B}\theta'' + f\phi' = 0 \tag{2.17}$$

Also the boundary conditions in (2.5) reduces to

$$f(0) = 0, f'(0) = 1, g(0) = -mf''(0), \theta(0) = \phi(0) = 1$$
$$f'(\infty) \to 0, g(\infty) \to 0, \theta(\infty) \to 0, \phi(\infty) \to 0 \tag{2.18}$$

The wall shear stress is given by

$$\tau_w = (\mu+k)\left(\frac{\partial u}{\partial y}\right)_{y=0} + kN_{y=0} \tag{2.19}$$

Friction factor is given by

$$C_{fx} = \frac{\tau_w}{(\rho u_w^2/2)} = 2\,\mathrm{Re}_x^{-1/2}\left(\frac{n+1}{2}\right)^{1/2}\left[(1+K)f''(0)+Kg(0)\right] \tag{2.20}$$

The wall couple stress is given by

$$M_w = \gamma\left(\frac{\partial N}{\partial y}\right)_{y=0} = \left(\frac{\gamma u_w^2}{\upsilon x}\right)\left(\frac{n+1}{2}\right)g'(0) \tag{2.21}$$

The dimensionless wall couple stress may be written as

$$M_w\left(\frac{\upsilon x}{\gamma u_w^2}\right) = \left(\frac{n+1}{2}\right)g'(0) \tag{2.22}$$

Heat transfer rate is given by

$$Nu_x = \frac{xq_w}{k_m(T_w - T_\infty)} = -\mathrm{Re}_x^{1/2}\left(\frac{n+1}{2}\right)^{1/2}\theta'(0) \tag{2.23}$$

Local Sherwood number is given by

$$Sh_x = \frac{xm_w}{D_B(C_w - C_\infty)} = -\mathrm{Re}_x^{1/2}\left(\frac{n+1}{2}\right)^{1/2}\phi'(0) \tag{2.24}$$

III. SOLUTION OF THE PROBLEM

The set of coupled non-linear governing boundary layer Equations (2.14) - (2.17) together with the boundary conditions (2.18) are solved numerically by using Runge-Kutta fourth order technique along with shooting method. First of all, higher order non-linear differential Equations (2.14) - (2.17) are converted into simultaneous linear differential equations of first order and they are further transformed into initial value problem by applying the shooting technique (Jain et al. [25]). The resultant initial value problem is solved by employing Runge-Kutta fourth order technique. The step size $\Delta\eta = 0.05$ is used to obtain the numerical solution with five decimal place accuracy as the criterion of convergence. From the process of numerical computation, the skin-friction coefficient, the wall couple stress, the Nusselt number and the Sherwood number, which are respectively proportional to $f''(0), g'(0), -\theta'(0)$ and $-\phi'(0)$, are also sorted out and their numerical values are presented in a tabular form.

IV. RESULTS AND DISCUSSIONS

The governing equations (2.14) - (2.17) subject to the boundary conditions (2.18) are integrated as described in section 3. In order to get a clear insight of the physical problem, the velocity, temperature and concentration have been discussed by assigning numerical values to the governing parameters encountered in the problem.

In order to assess the accuracy of the results, we compared our results for $R=Q=N_T=N_B=0$ with literature data from Gorla and Kumari [4] in Table I and found that they are in excellent agreement. This suggests that the present results are accurate. Tables' II–X present data for friction factor, heat and mass transfer rates for parametric values of variables governing the problem. Thermophoresis parameter, N_T appears in the thermal and concentration boundary layer equations. As we note, it is coupled with temperature function and plays a strong role in determining the diffusion of heat and nanoparticle concentration in the boundary layer. Table II shows that as the thermophoresis parameter increases, friction factor increase, where as the heat and mass transfer rates decrease. N_B is the Brownian motion parameter. Brownian motion decelerates the flow in the nanofluid boundary layer. Brownian diffusion promotes heat conduction. The nanoparticles increase the surface area for heat transfer. Nanofluid is a two phase fluid where the nanoparticles move randomly and increase the energy exchange rates. Brownian motion reduces nanoparticle diffusion. Table III shows that as the Brownian motion parameter N_B increases, mass transfer rate increase, whereas the friction factor and heat transfer rate decrease. Table IV shows that as the power law exponent n increases, heat transfer rate increases whereas friction factor and mass transfer rate decrease. Table V shows that as the parameter S increases, friction factor, heat and mass transfer rates increases. Table VI shows that as the vortex viscosity parameter K increases, the friction factor, and the heat and mass transfer rates increases. Table VII shows that friction factor, heat and mass transfer rates increases with the buoyancy parameter λ. Table VIII shows that as the Schmidt number increases, the friction factor and mass transfer rates increase. Table IX shows that as the constant m increases, the wall friction, heat and mass transfer rates decreases. The value m=0 represents concentrated particle flows in which the particle density is sufficiently great that microelements close to the wall are unable to rotate. This condition is also called as the strong interaction. When m = 0.5 the particle rotation is equal to fluid viscosity at the boundary for one particle suspension. When m = 1, we have flows which are representative to turbulent boundary layers. Table X shows that as the radiation and heat source/sink parameters increases, the friction factor and mass transfer rate increase, where as heat transfer rate decreases.

Figures 1(a)-1(d) and 2(a)-2(d) show the effect of the thermophoresis number, N_T as well as the Brownian motion parameter, N_B on velocity, angular velocity, temperature and concentration profiles. As N_T increases, velocity, angular velocity, temperature and concentration within the boundary layer increase. As N_B increases, temperature increases whereas the velocity, angular velocity and concentration decrease within the boundary layer. Figure 3(a)-3(d) shows that as the exponent n increases, velocity decreases whereas the angular velocity, temperature and concentration increase. The effects of the parameter S on the boundary layer profiles are opposite to the effects of n as seen from Figure 4(a)-4(d). Figures 5(a)-5(d) and 6(a)-6(d) show that as the vortex viscosity parameter K increases, the velocity and angular velocity increases whereas the temperature and concentration within the boundary layer decrease. As the mixed convection parameter λ increases, the velocity increases whereas the angular velocity, temperature and concentration within the boundary layer decrease. Figure 7(a)-7(d) shows that as the Prandtl number Pr increases, velocity and temperature decreases whereas the angular velocity and concentration increase. As the Schmidt number increases, the velocity and concentration boundary layer thickness decreases whereas angular velocity and temperature increase. This is seen from Figure 8(a)-8(d). As the constant m increases, the velocity decreases whereas the angular velocity, temperatures and concentration increases. This is seen from Figure 9(a)-9(d). Figures 10(a)-10(d) and 11(a)-11(d) shows that as the radiation parameter R and heat source/sink parameter Q increases, angular velocity decreases whereas velocity, temperature and concentration increase.

Table I: Numerical values of $(1+K/2)f''(0)$ *and* $-\theta'(0)$ at the sheet for different values of K *and* n when $\lambda = 1.0, S = N_T = N_B = R = Q = 0.0, m = 0.5$ and *Pr=0.72*, Comparison of the present results with that of Gorla and Kumari [4]

K	n	Present results		Gorla and Kumari [4]	
		$(1+K/2)f''(0)$	$-\theta'(0)$	$(1+K/2)f''(0)$	$-\theta'(0)$
0.0	0.50	-0.129346	0.586095	-0.129016	0.584934
0.0	0.75	-0.312889	0.568677	-0.311993	0.567454
0.0	1.00	-0.444373	0.555571	-0.443205	0.554359
0.0	1.50	-0.621160	0.536891	-0.619938	0.535696
0.0	3.00	-0.874189	0.507159	-0.873003	0.505097
1.0	0.50	-0.293989	0.593002	-0.292302	0.592127
1.0	0.75	-0.497473	0.577915	-0.495675	0.577132
1.0	1.00	-0.643706	0.566632	-0.641769	0.565834
1.0	1.50	-0.840768	0.550693	-0.838697	0.549797
1.0	3.00	-1.123040	0.525838	-1.121011	0.524109

Table II: Numerical values of $f''(0), g'(0), -\theta'(0)$ *and* $-\phi'(0)$ at the sheet for different values of N_T when $K = S = \lambda = 1, N_B = 0.3, m = 0.5, Q = 0.2, n = 2, \Pr = 10$ and Sc=10.

N_T	$f''(0)$	$g'(0)$	$-\theta'(0)$	$-\phi'(0)$
0.1	-0.664881	-0.243793	1.065830	2.26034
0.2	-0.655741	-0.239314	1.045970	2.16199
0.3	-0.646809	-0.234939	1.026430	2.07338
0.4	-0.638081	-0.230668	1.007200	1.99418
0.5	-0.629554	-0.226498	0.988283	1.92407

Table III: Numerical values of $f''(0), g'(0), -\theta'(0)$ *and* $-\phi'(0)$ at the sheet for different values of N_B when $K = S = \lambda = 1, N_T = 0.3, m = 0.5, Q = 0.2, n = 2, \Pr = 10$ and Sc=10.

N_B	$f''(0)$	$g'(0)$	$-\theta'(0)$	$-\phi'(0)$
0.1	-0.599733	-0.211426	1.111610	1.30727
0.2	-0.635423	-0.229303	1.065070	1.88328
0.3	-0.646809	-0.234939	1.026430	2.07338
0.4	-0.652032	-0.237504	0.990473	2.16771
0.5	-0.654779	-0.238841	0.956098	2.22387

Table IV: Numerical values of $f''(0), g'(0), -\theta'(0)$ *and* $-\phi'(0)$ at the sheet for different values of n when $K = S = R = \lambda = 1, N_T = N_B = 0.3, m = 0.5, Q = 0.2, \Pr = 10$ and Sc=10.

n	$f''(0)$	$g'(0)$	$-\theta'(0)$	$-\phi'(0)$
0.5	-0.197829	0.172956	1.00874	2.20583
1.0	-0.430952	-0.0263596	1.06582	2.10284
1.5	-0.563788	-0.15134	1.10126	2.04072
2.0	-0.649813	-0.23634	1.12576	1.99916
3.0	-0.754761	-0.344031	1.15695	1.94704
5.0	-0.857058	-0.452846	1.18866	1.89471

Table V: Numerical values of $f''(0), g'(0), -\theta'(0)$ *and* $-\phi'(0)$ at the sheet for different values of S when $K = \lambda = R = 1, N_T = N_B = 0.3, m = 0.5, Q = 0.2, n = 2, \Pr = 10$ and Sc=10.

S	$f''(0)$	$g'(0)$	$-\theta'(0)$	$-\phi'(0)$
0.5	-0.705108	-0.267333	1.11713	1.99127
0.6	-0.694000	-0.261128	1.11888	1.99287
0.7	-0.682917	-0.254928	1.12062	1.99445
0.8	-0.671858	-0.248728	1.12234	1.99603
0.9	-0.660824	-0.242532	1.12406	1.99760
1.0	-0.649813	-0.230340	1.12576	1.99916

Table VI: Numerical values of $f''(0), g'(0), -\theta'(0)$ *and* $-\phi'(0)$ at the sheet for different values of K when $S = \lambda = R = 1, N_T = N_B = 0.3, m = 0.5, Q = 0.2, n = 2, \Pr = 10$ and Sc=10.

K	$f''(0)$	$g'(0)$	$-\theta'(0)$	$-\phi'(0)$
0.0	-0.708256	-0.368713	0.99671	2.05477
0.5	-0.678646	-0.284347	1.01363	2.06507
1.0	-0.646809	-0.234939	1.02043	2.07338
2.0	-0.593866	-0.176569	1.04481	2.08581
3.0	-0.554020	-0.142405	1.05753	2.09470

Table VII: Numerical values of $f''(0), g'(0), -\theta'(0)$ *and* $-\phi'(0)$ at the sheet for different values of λ when $K = S = R = 1, N_T = N_B = 0.3, m = 0.5, Q = 0.2, n = 2, \Pr = 10$ and Sc=10.

λ	$f''(0)$	$g'(0)$	$-\theta'(0)$	$-\phi'(0)$
0.0	-0.902584	-0.3743770	0.976165	2.03765
0.5	-0.772424	-0.3042750	1.002770	2.05617
1.0	-0.646809	-0.2349390	1.026430	2.07338
1.5	-0.524913	-0.1662230	1.047850	2.08950
2.0	-0.406157	-0.0980246	1.087500	2.10473

Table VIII: Numerical values of $f''(0), g'(0), -\theta'(0)$ *and* $-\phi'(0)$ at the sheet for different values of λ when $K = S = R = 1, N_T = N_B = 0.3, m = 0.5, Q = 0.2, n = 2, \Pr = 10$ and Sc=10.

Sc	$f''(0)$	$g'(0)$	$-\theta'(0)$	$-\phi'(0)$
1	-0.444950	-0.144039	1.27846	-0.185624
10	-0.649813	-0.236340	1.12596	1.999160
20	-0.683747	-0.254022	1.10025	3.160030
50	-0.714107	-0.270606	1.08001	5.353600
100	-0.729246	-0.279186	1.07134	7.757390

Table IX: Numerical values of $f''(0), g'(0), -\theta'(0)$ *and* $-\phi'(0)$ at the sheet for different values of m when $K = S = \lambda = R = 1, N_T = N_B = 0.3, Q = 0.2, n = 2, \Pr = 10$ and Sc=10.

m	$f''(0)$	$g'(0)$	$-\theta'(0)$	$-\phi'(0)$
0.0	-0.556371	0.175433	1.14406	2.01556
0.5	-0.649813	-0.23634	1.12576	1.99916
1.0	-0.781214	-0.805276	1.09812	1.97507

Table X: Numerical values of $f''(0), g'(0), -\theta'(0)$ *and* $-\phi'(0)$ at the sheet for different values of R and Q when $K = S = \lambda = 1, N_T = N_B = 0.3, m = 0.5, n = 2, \Pr = 10$ and Sc=10.

R	Q	$f''(0)$	$g'(0)$	$-\theta'(0)$	$-\phi'(0)$
0	0.2	-0.677021	-0.248789	1.420510	1.885870
1	0.2	-0.646809	-0.234939	1.026430	2.073380
2	0.2	-0.624100	-0.225284	0.825949	2.165100
3	0.2	-0.605761	-0.217902	0.701209	2.219370
1	-0.5	-0.664790	-0.243369	1.701410	1.556840
1	0.0	-0.655018	-0.238772	1.308890	1.308890
1	0.5	-0.639733	-0.231650	0.807817	2.234470

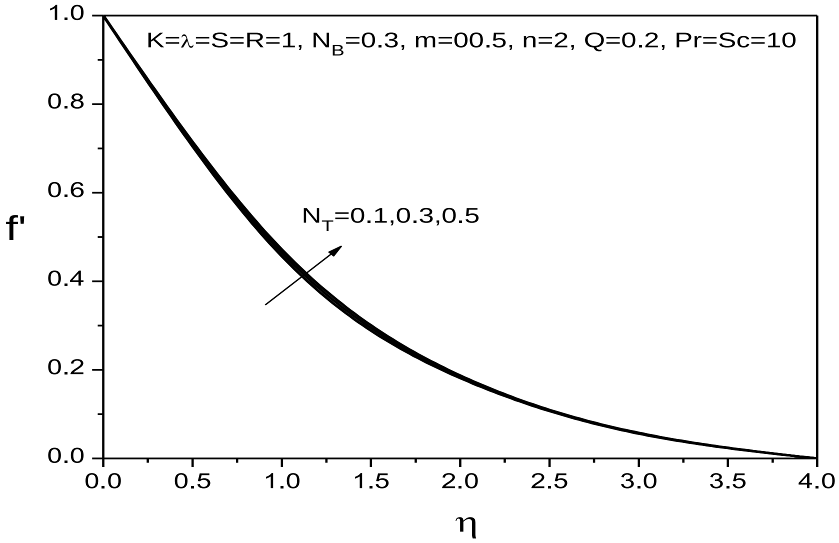

Fig.1(a) Velocity profiles for different values of N_T

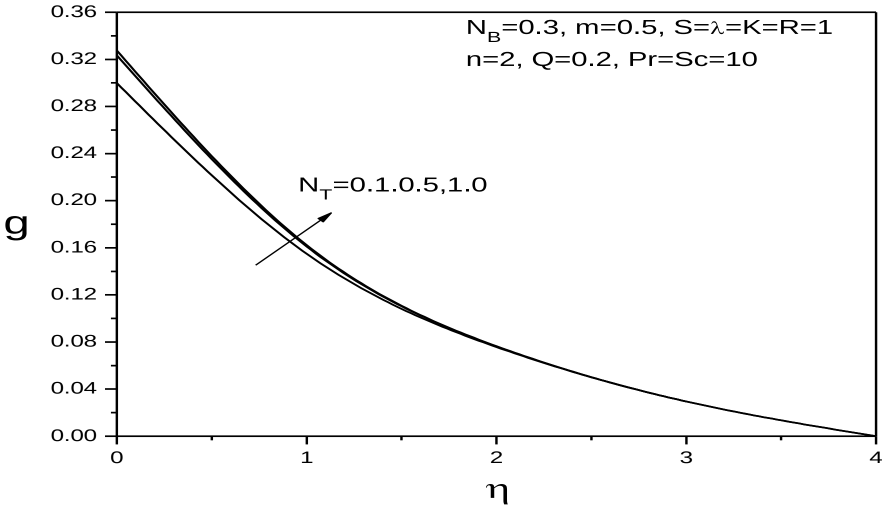

Fig.1(b) Angular velocity profiles for different values of N_T

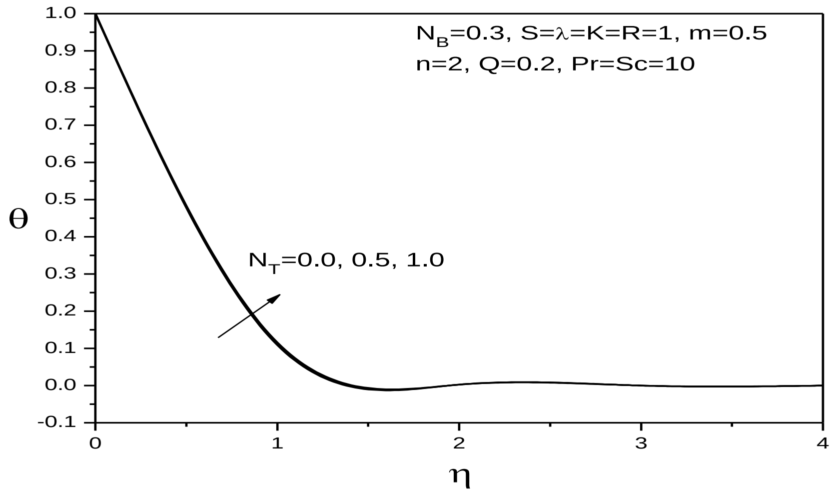

Fig.1(c) Temperature profiles for different values of N_T

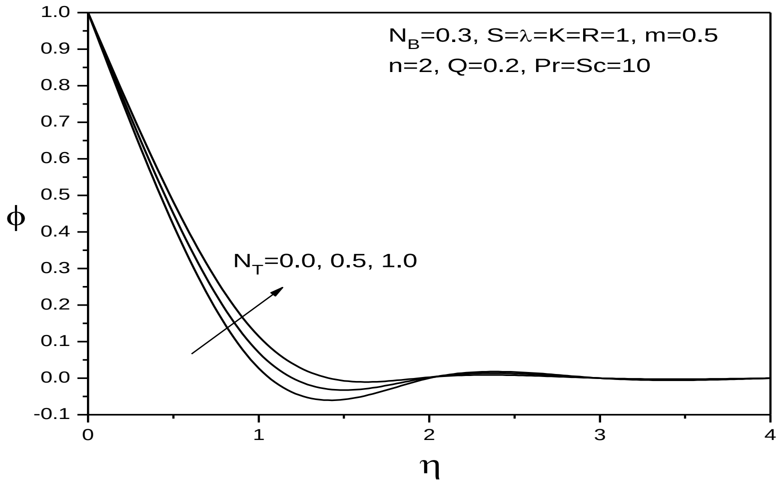

Fig.1(d) Concentration profiles for different values of N_T

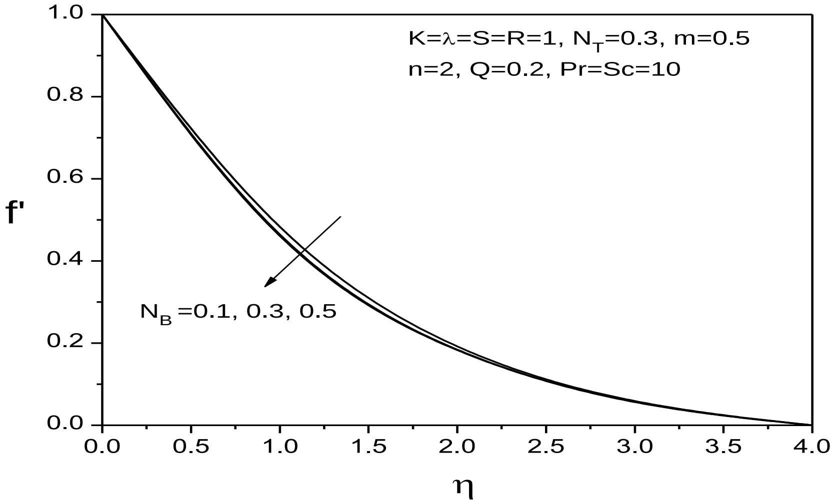

Fig.2(a) Velocity profiles for different values of N_B

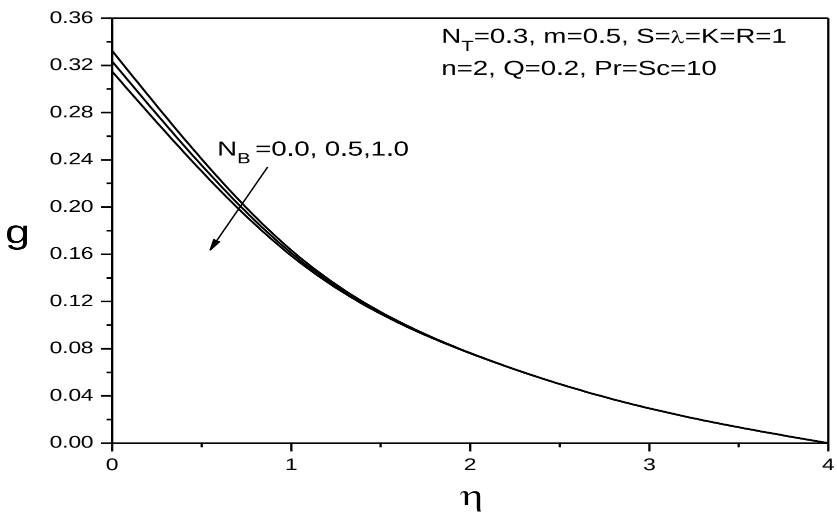

Fig.2(b) Angular velocity profiles for different values of N_B

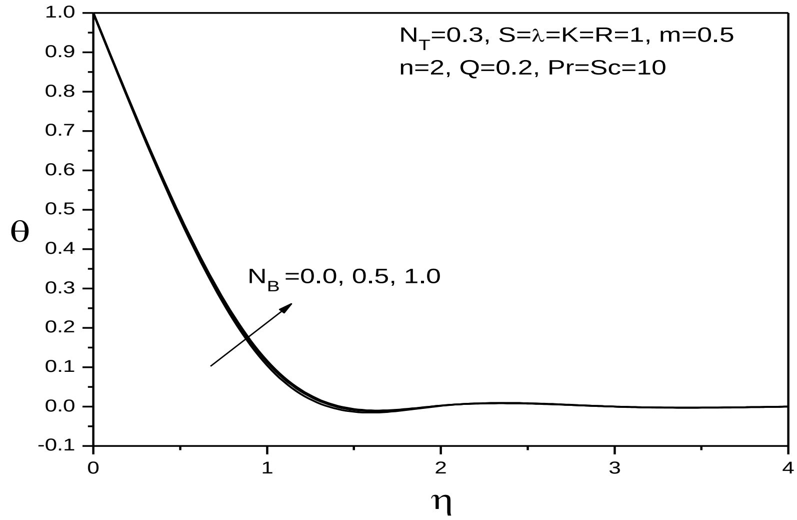

Fig.2(c) Temperature profiles for different values of N_B

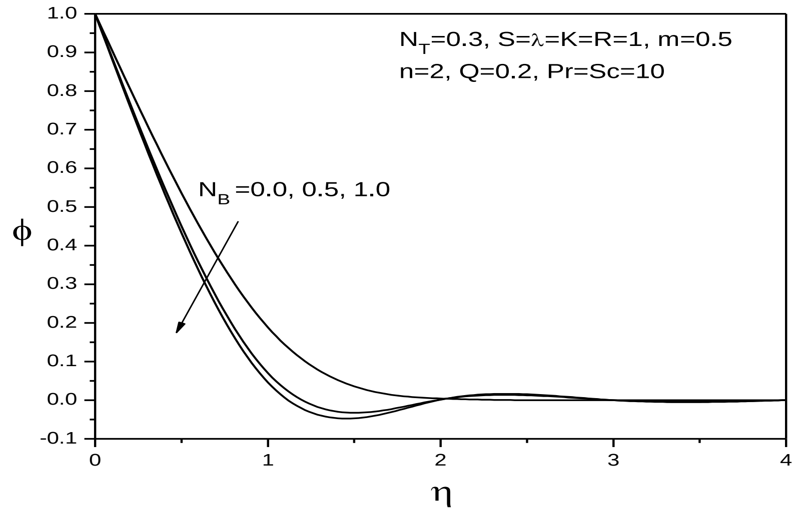

Fig.2(d) Concentration profiles for different values of N_B

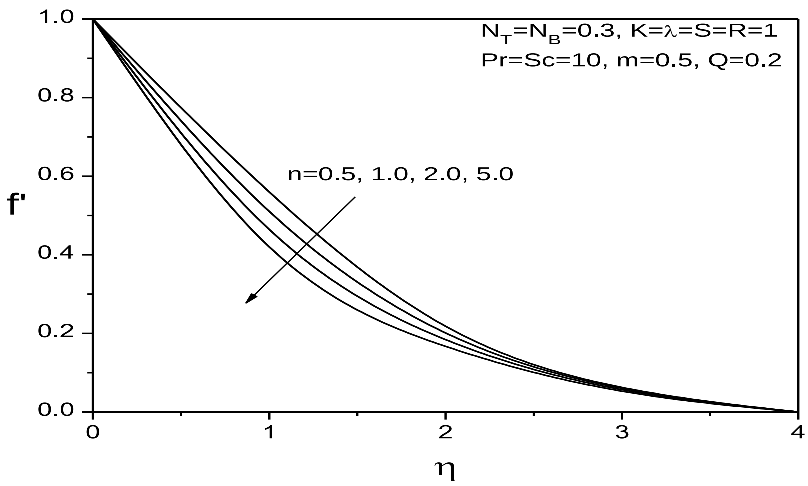

Fig.3(a) Velocity profiles for different values of n

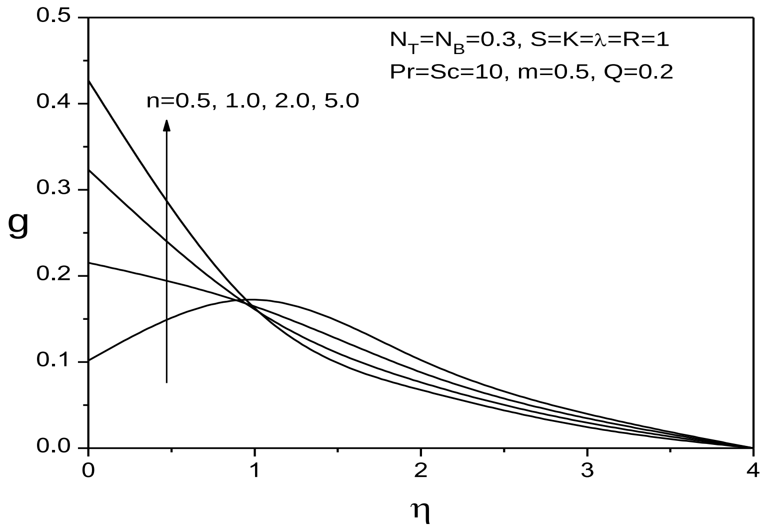

Fig.3(b) Angular velocity profiles for different values of *n*

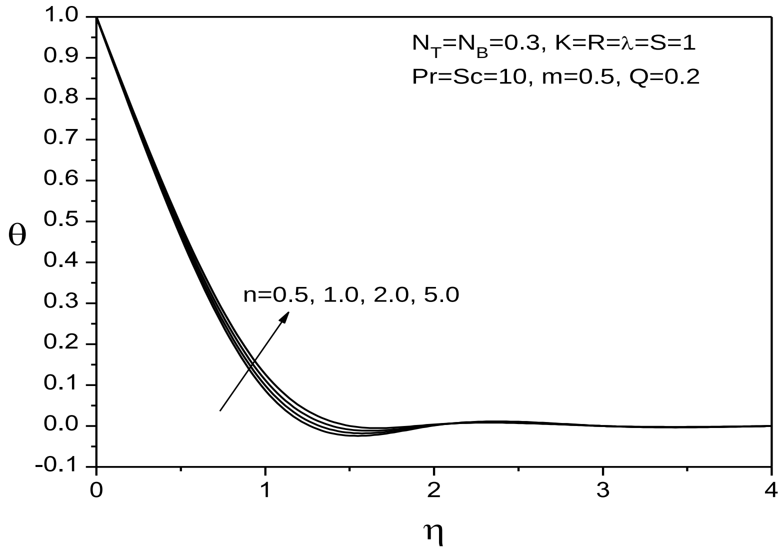

Fig.3(c) Temperature profiles for different values of *n*

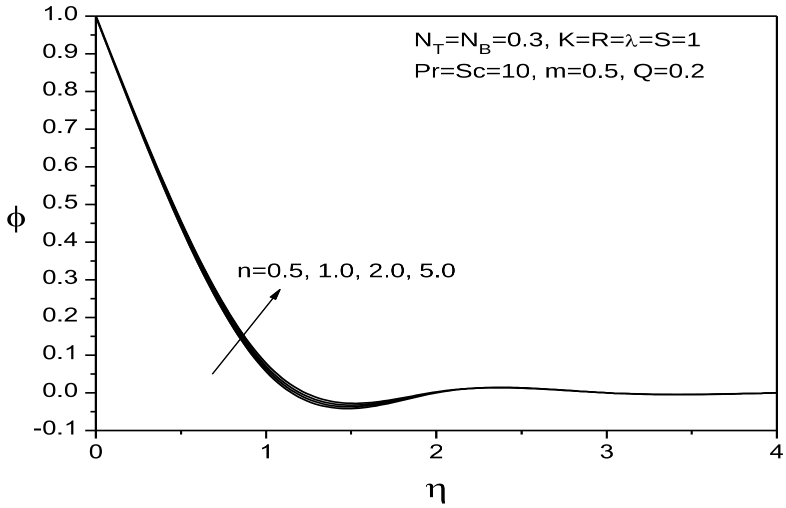

Fig.3(d) Concentration profiles for different values of *n*

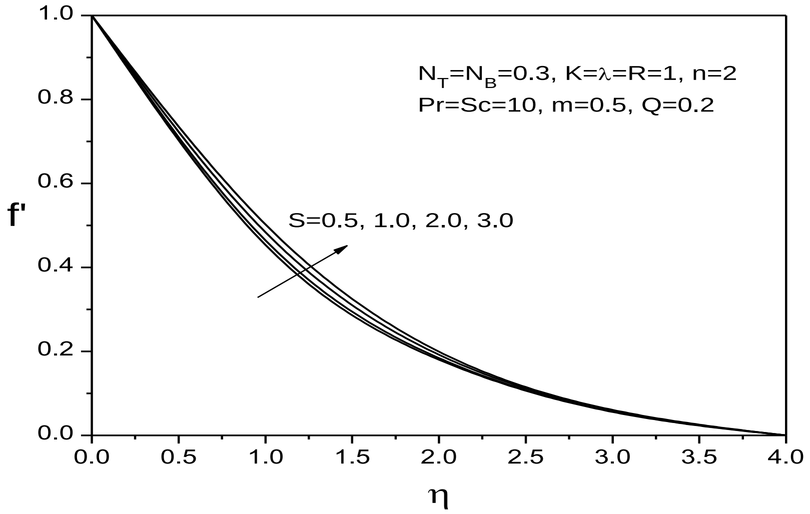

Fig.4(a) Velocity profiles for different values of *S*

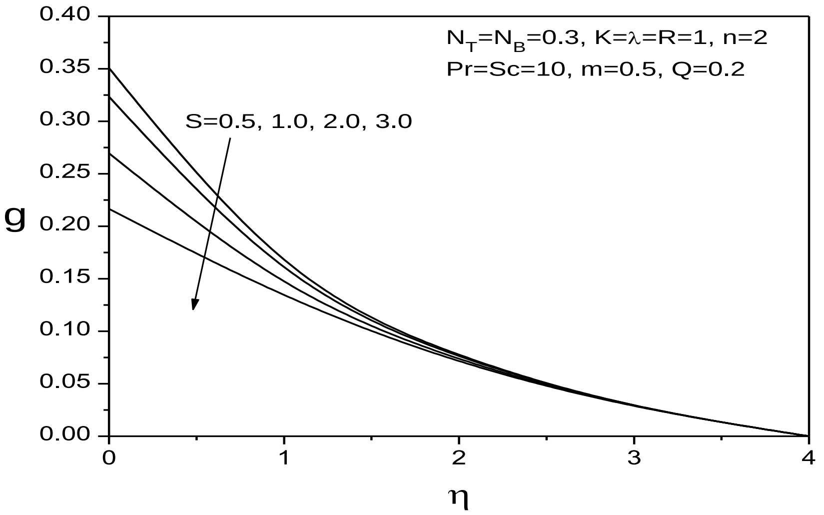

Fig.4(b) Angular velocity profiles for different values of *S*

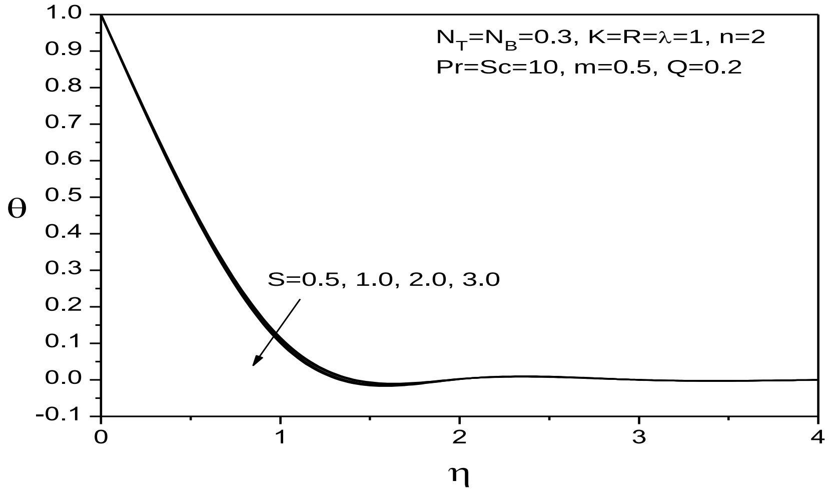

Fig.4(c) Temperature profiles for different values of *S*

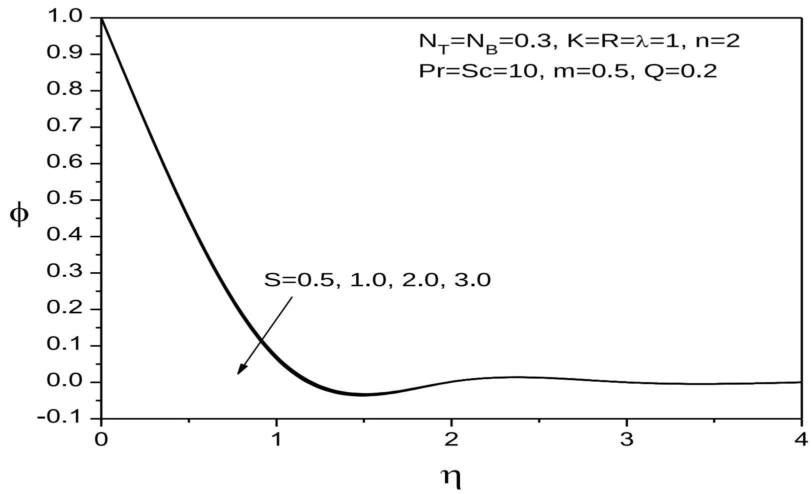

Fig.4(d) Concentration profiles for different values of *S*

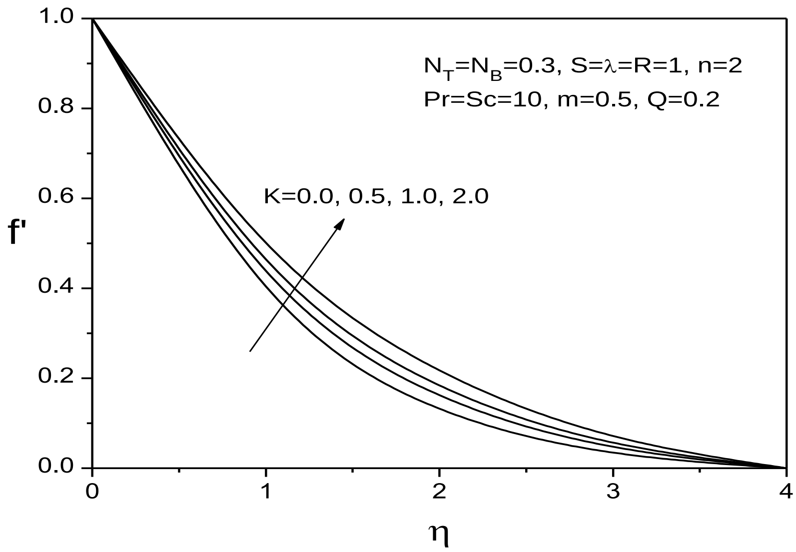

Fig.5(a) Velocity profiles for different values of *K*

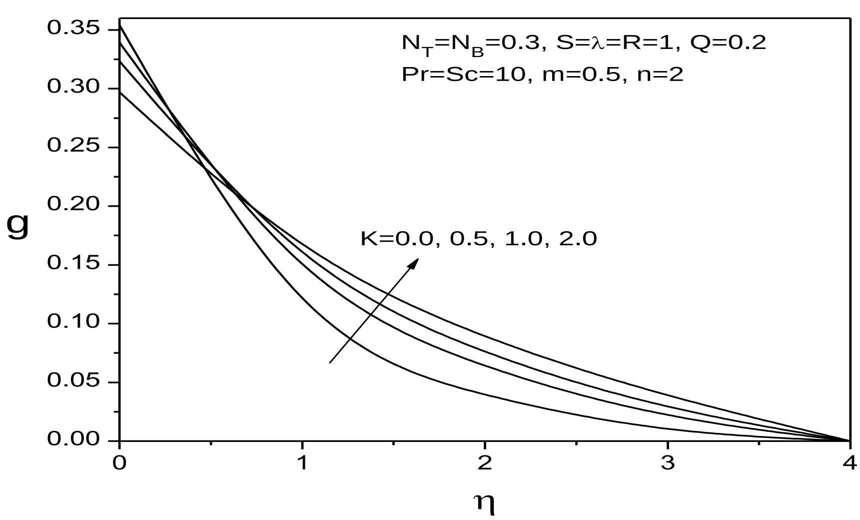

Fig.5(b) Angular velocity profiles for different values of *K*

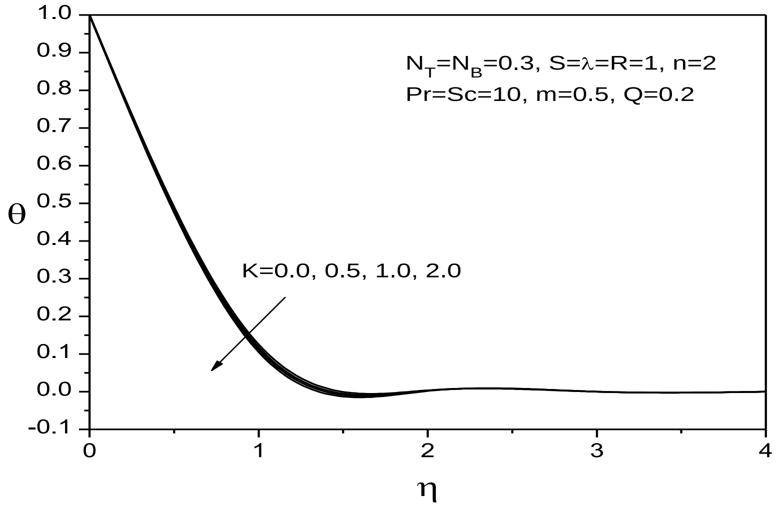

Fig.5(c) Temperature profiles for different values of *K*

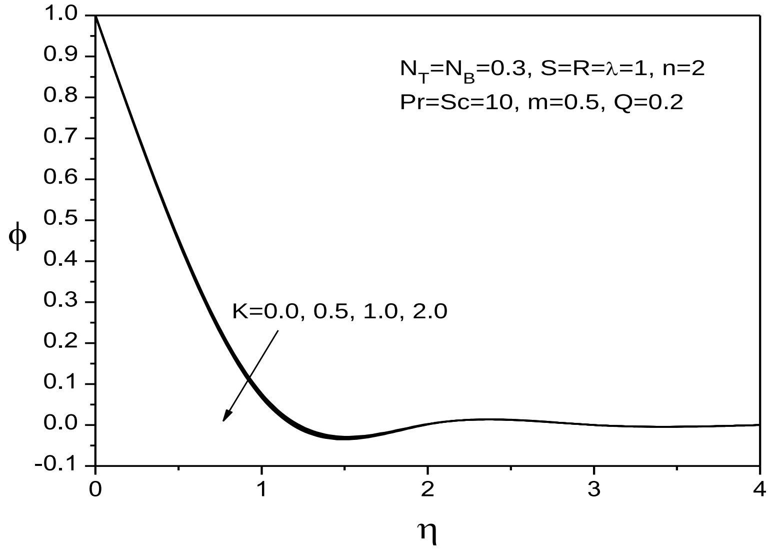

Fig.5(d) Concentration profiles for different values of *K*

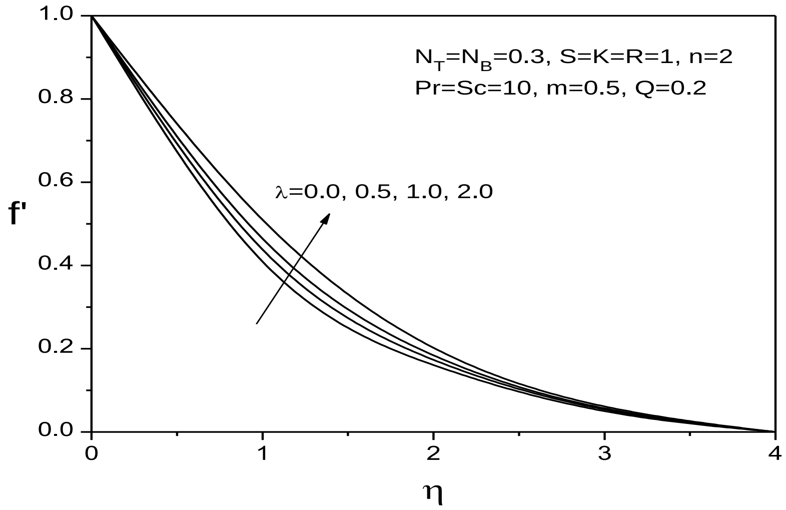

Fig.6(a) Velocity profiles for different values of λ

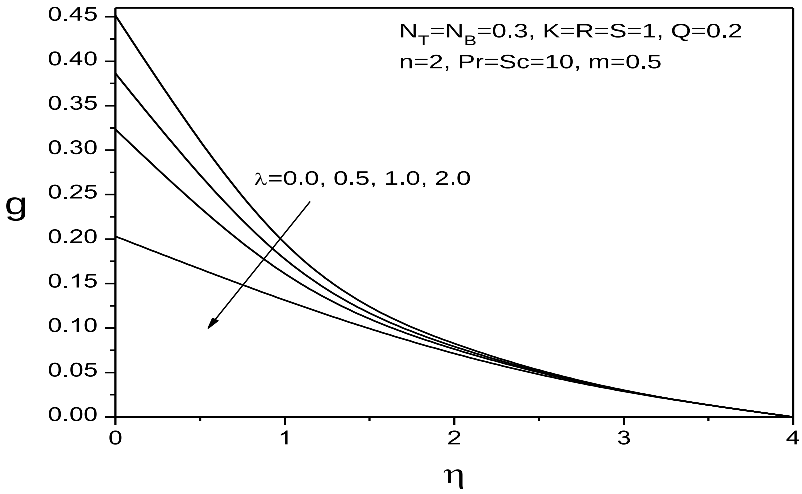

Fig.6(b) Angular velocity profiles for different values of λ

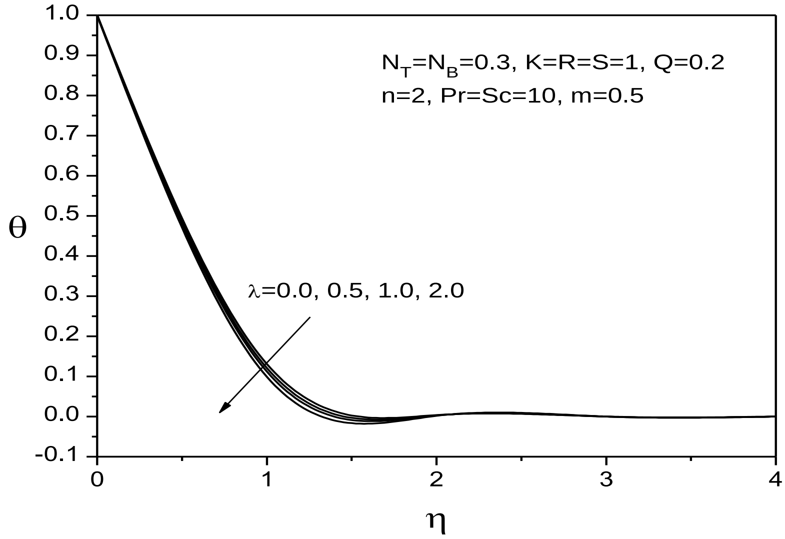

Fig.6(c) Temperature profiles for different values of λ

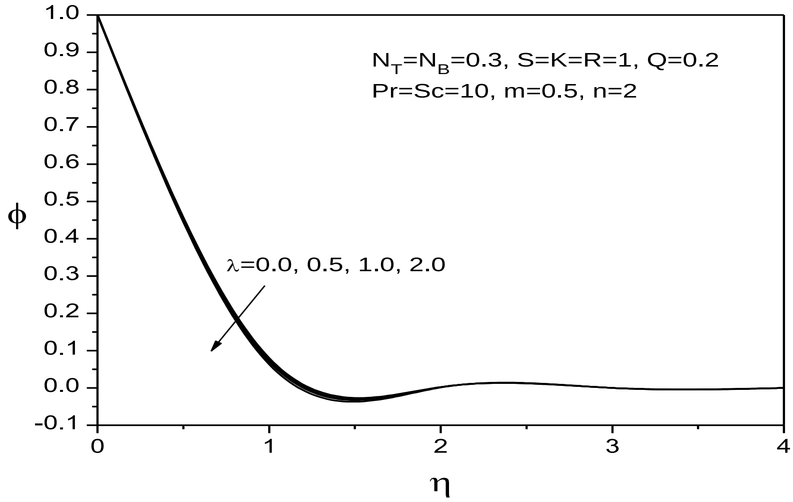

Fig.6(d) Concentration profiles for different values of λ

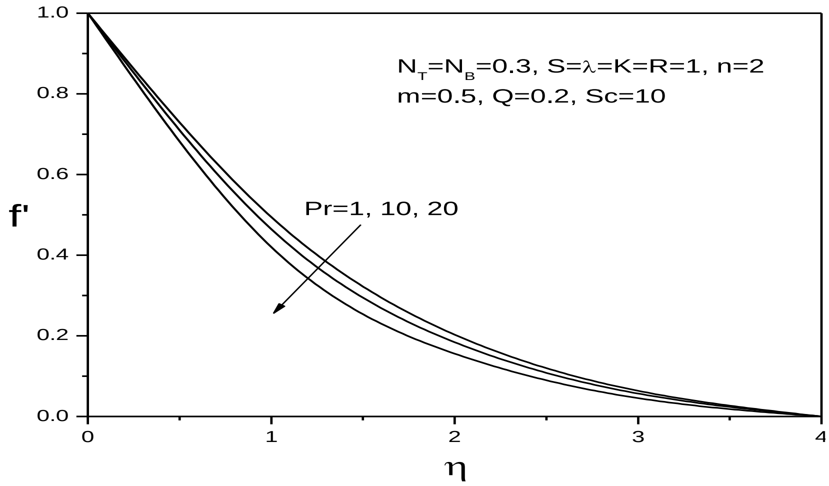

Fig.7(a) Velocity profiles for different values of *Pr*

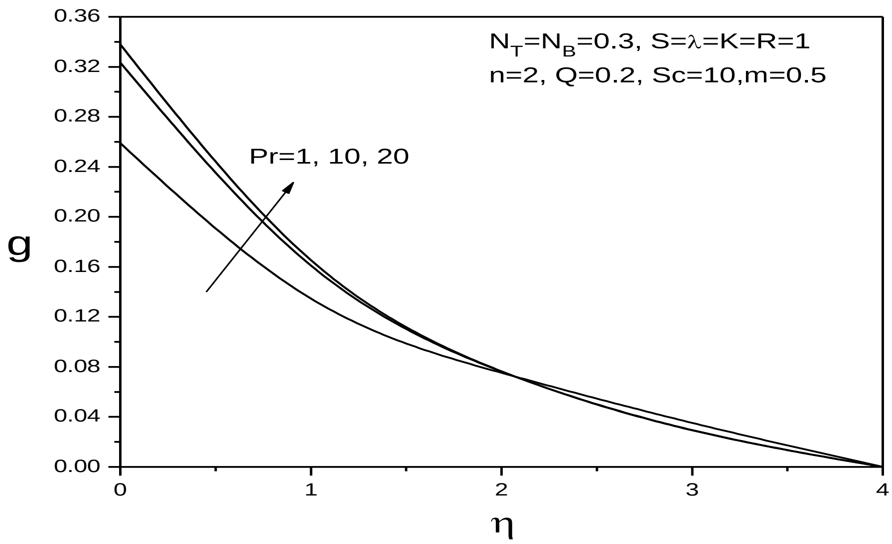

Fig.7(b) Angular velocity profiles for different values of *Pr*

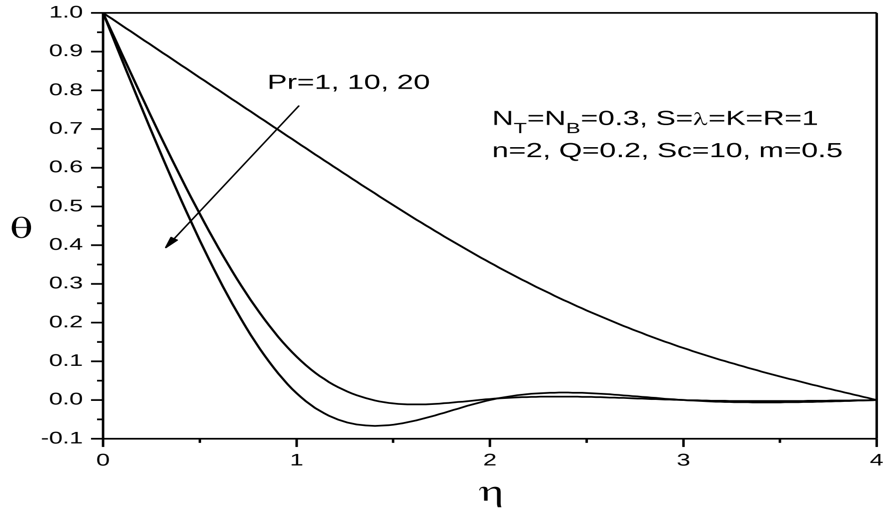

Fig.7(c) Temperature profiles for different values of *Pr*

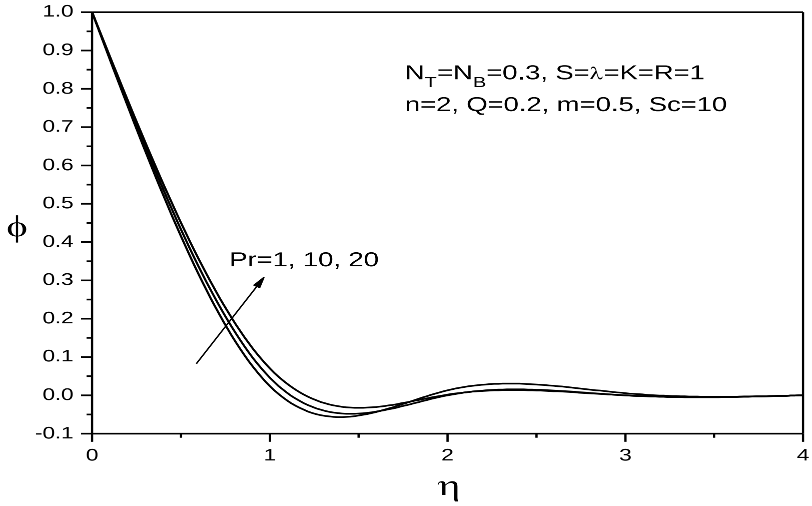

Fig.7(d) Concentration profiles for different values of *Pr*

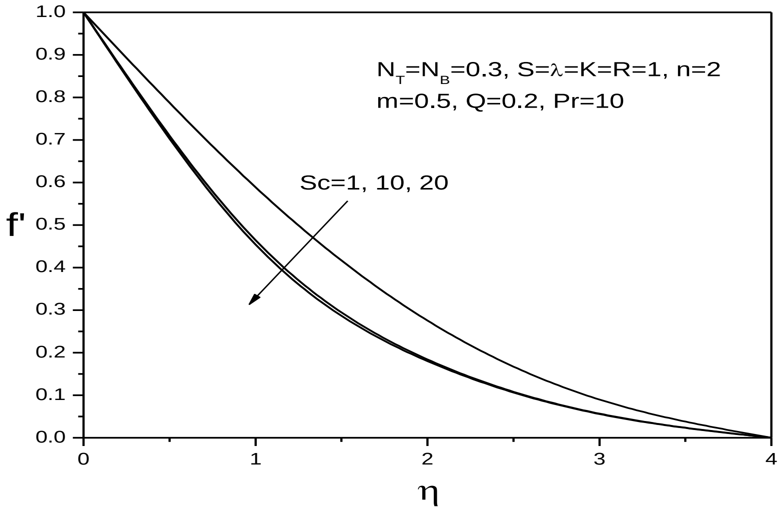

Fig.8(a) Velocity profiles for different values of *Sc*

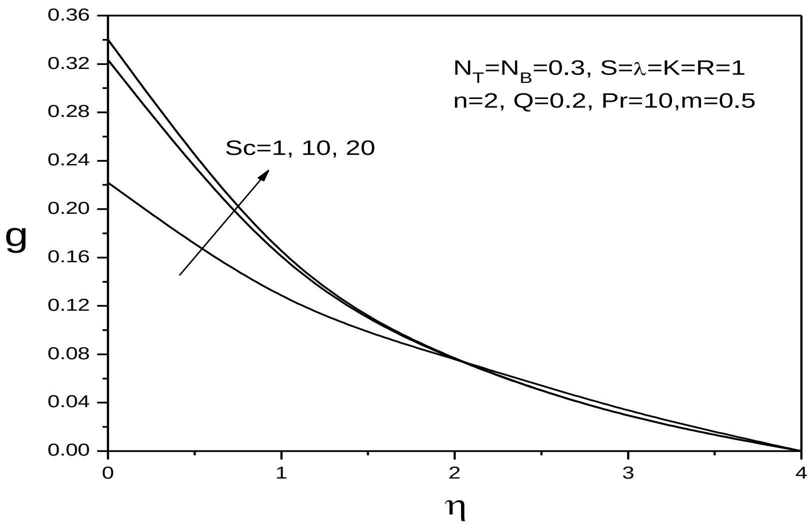

Fig.8(b) Angular velocity profiles for different values of *Sc*

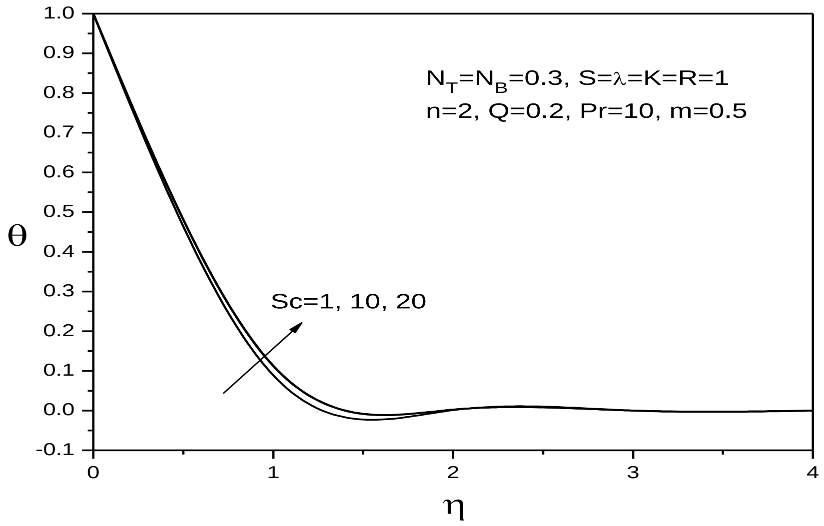

Fig.8(c) Temperature profiles for different values of *Sc*

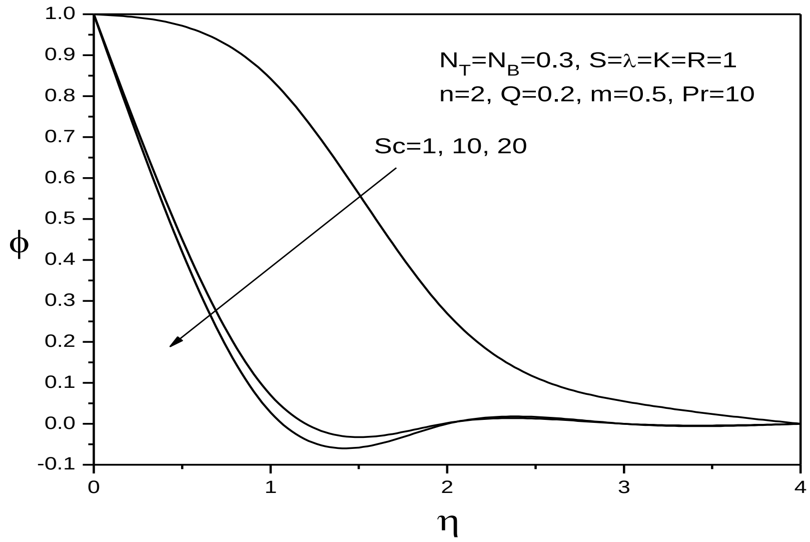

Fig.8(d) Concentration profiles for different values of *Sc*

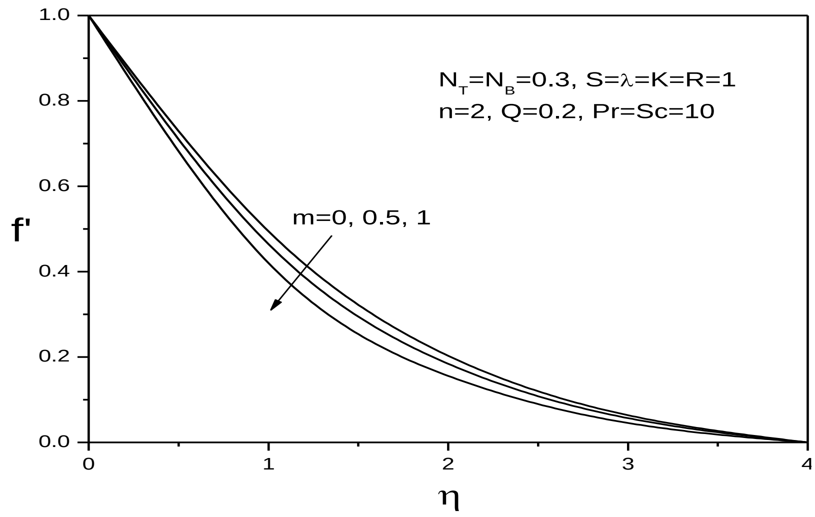

Fig.9(a) Velocity profiles for different values of *m*

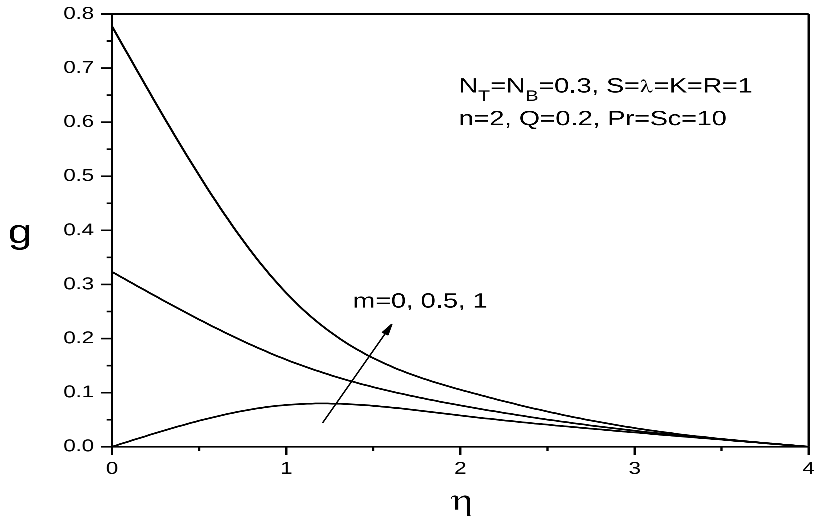

Fig.9(b) Angular velocity profiles for different values of *m*

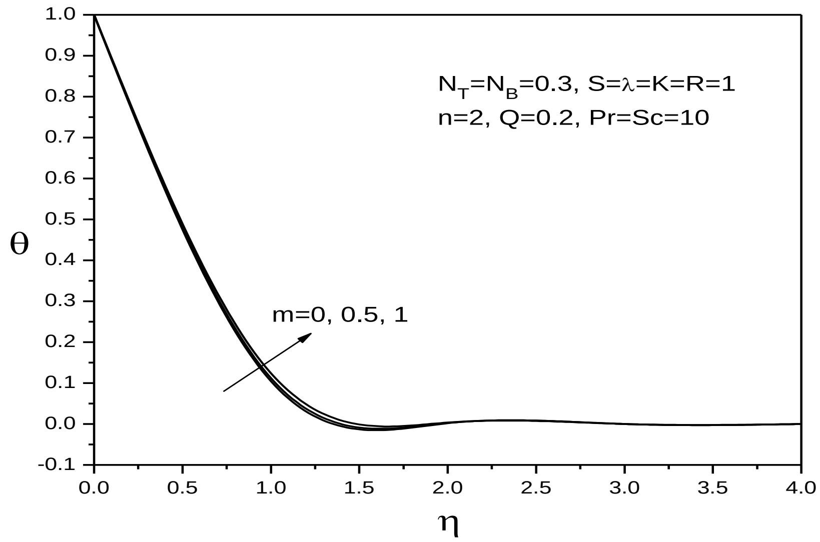

Fig.9(c) Temperature profiles for different values of *m*

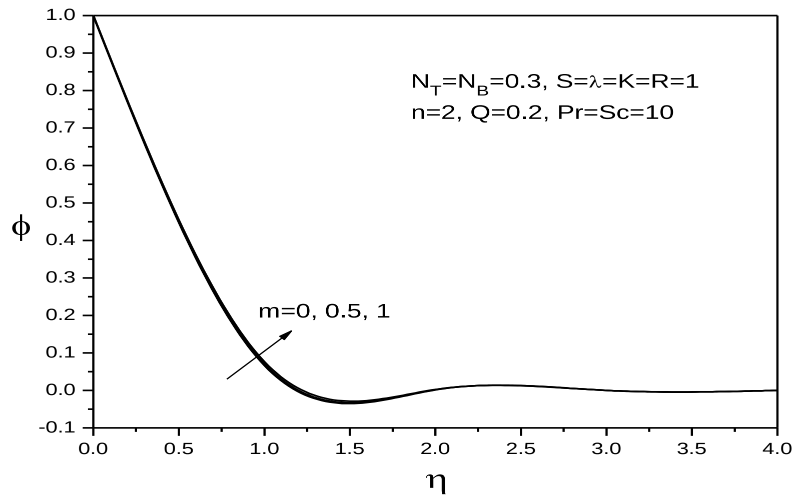

Fig.9(d) Concentration profiles for different values of *m*

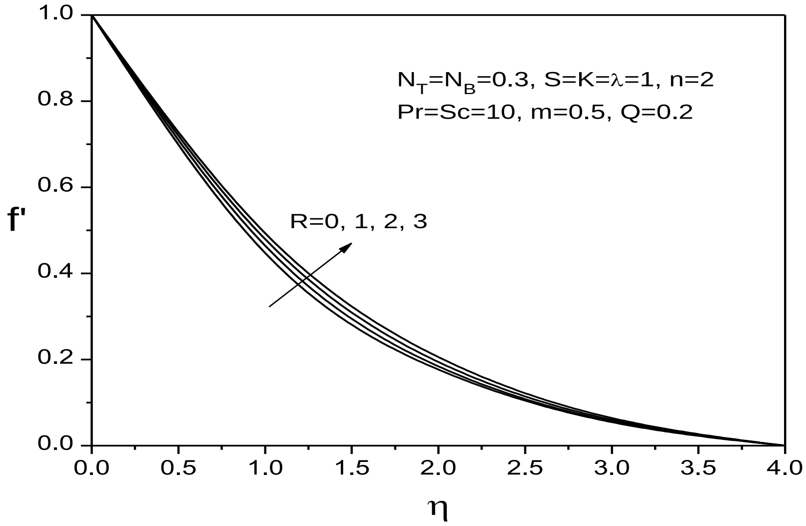

Fig.10(a) Velocity profiles for different values of *R*

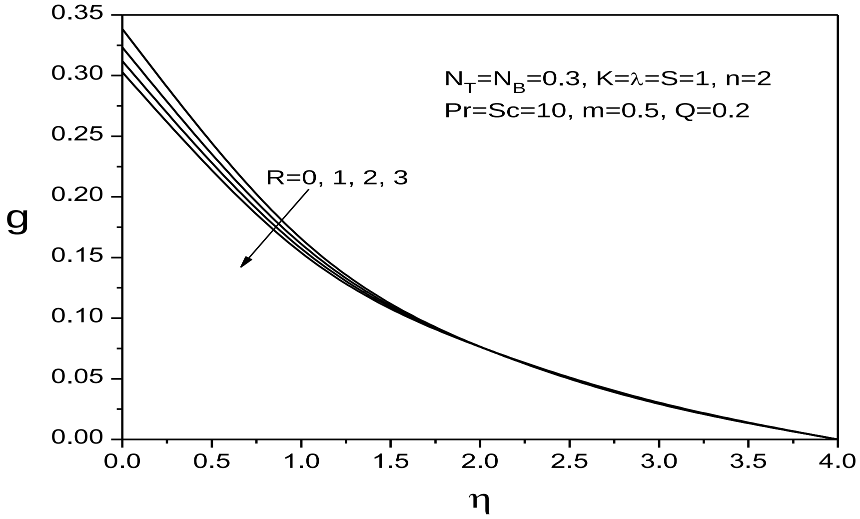

Fig.10(b) Angular velocity profiles for different values of *R*

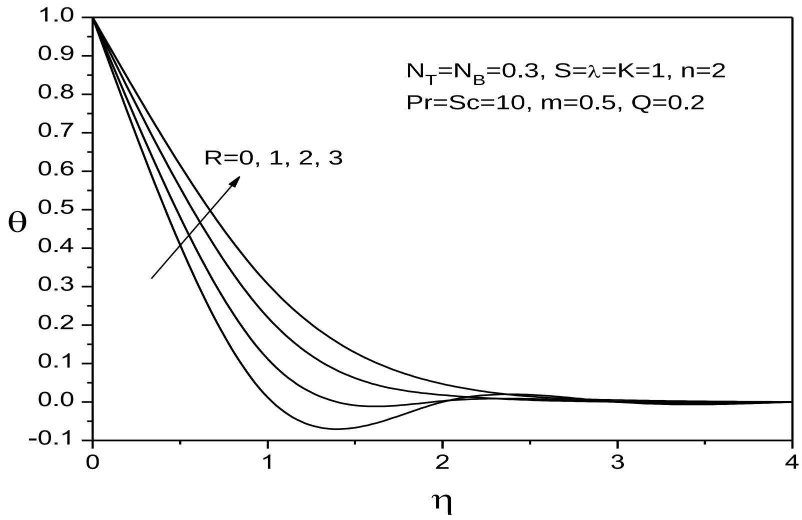

Fig.10(c) Temperature profiles for different values of *R*

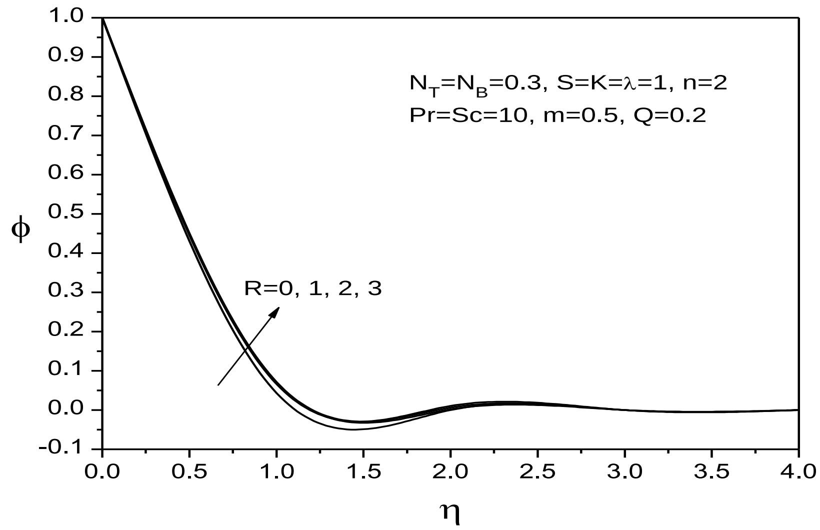

Fig.10(d) Concentration profiles for different values of *R*

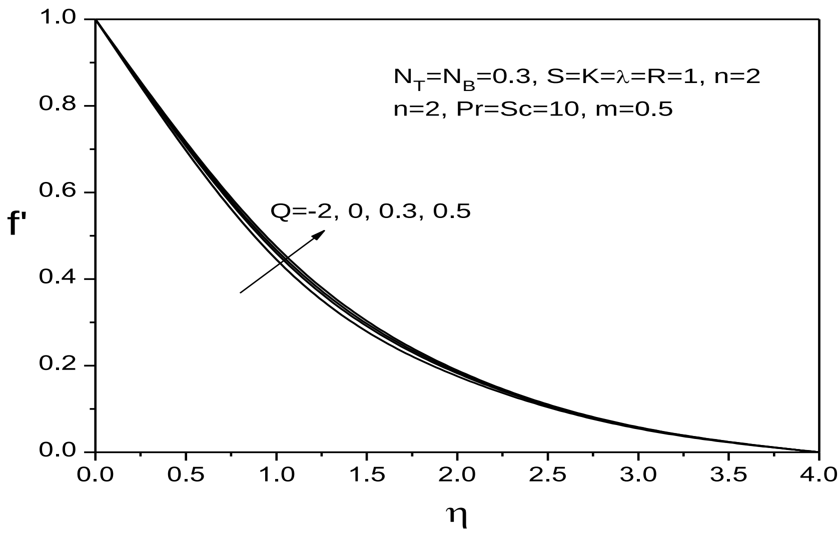

Fig.11(a) Velocity profiles for different values of *Q*

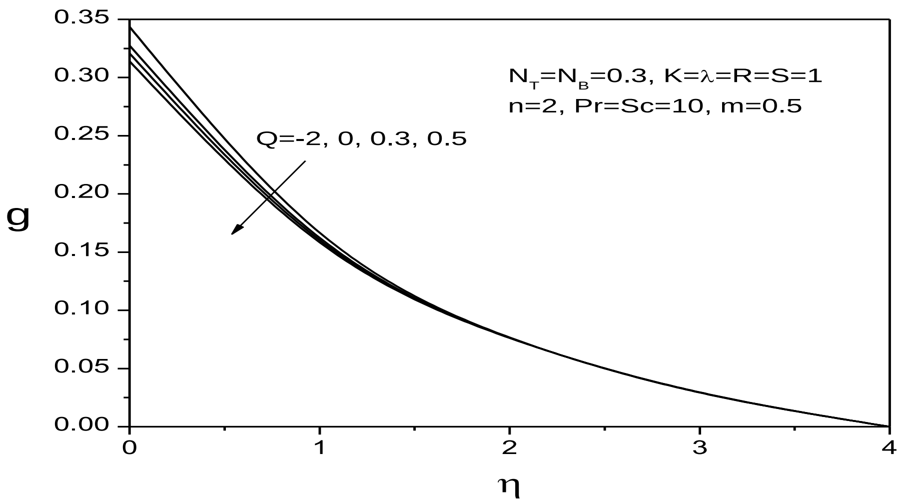

Fig.11(b) Angular velocity profiles for different values of *Q*

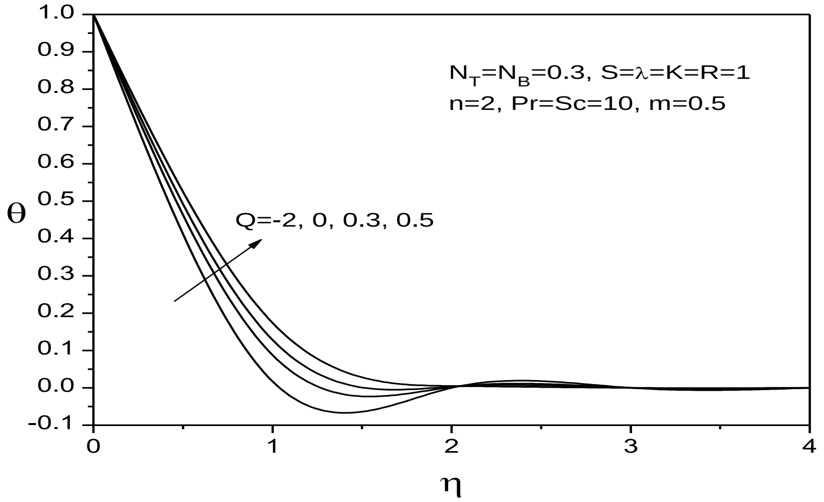

Fig.11(c) Temperature profiles for different values of *Q*

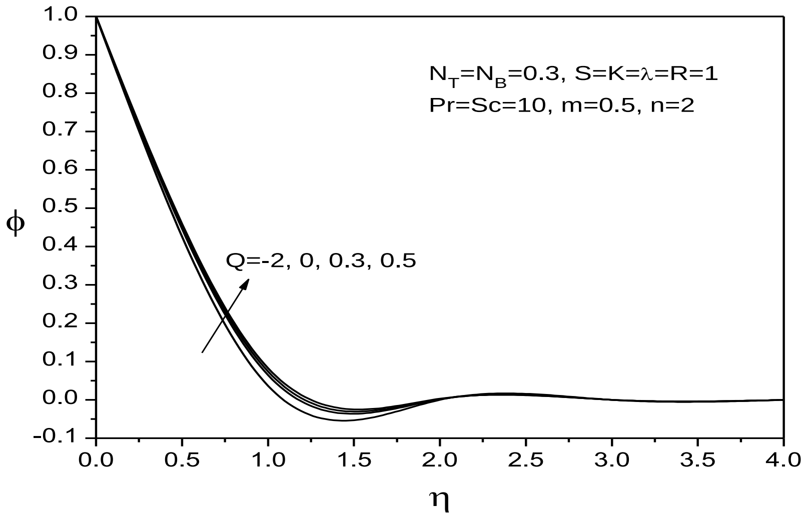

Fig.11(d) Concentration profiles for different values of *Q*

V. CONCLUSIONS

In this paper, we have presented a boundary layer analysis for the mixed convection flow of a non-Newtonian nanofluid on a non-linearly stretching sheet by taking radiation and heat source/sink into account. The micropolar model is chosen for the non-Newtonian fluid since the spinning motion of the nanoparticles as they move along the streamwise direction can be best described by the micropolar fluid model. The governing boundary layer equations have been transformed to a two-point boundary value problem in similarity variables and the resultant problem is solved numerically using the fourth order Runga-Kutta method along with shooting technique. The particular solutions reported in this paper were validated by comparing with solutions existing in the previously published paper. Our results show a good agreement with the existing work in the literature. The results are summarized as follows

1. The thermophoresis parameter increases, friction factor increase, where as the heat and mass transfer rates decreases.
2. Brownian motion reduces nanoparticle diffusion.
3. The radiation and heat source/sink increases the friction factor and mass transfer rate and reduces the heat transfer rate.
4. The radiation and heat source/sink reduces the angular velocity, and increase the velocity, temperature and concentration.

REFERENCES

1 Pearson, J. R. A., Tardy, P. M. J, (2002), Models for flow of non-Newtonian and complex fluids through porous media, J Non Newton Fluid Mech, Vol.102, pp.447–473.
2 Ellahi R, Afza, S, (2009), Effects of variable viscosity in a third grade fluid with porous medium: an analytic solution, Commun Nonlinear Sci Numer Simul., Vol.14(5), pp.2056–2072.
3 Ellahi, R, (2009), Effects of the slip boundary condition on non- Newtonian flows in a channel, Commun Nonlinear Sci Numer Simul., Vol.144, pp.1377–1384.

4 Rama Subba Reddy Gorla and Mahesh Kumari, (2012), Mixed Convection Flow of a Non-Newtonian Nanofluid Over a Non-Linearly Stretching Sheet, Journal of Nanofluids, Vol. 1, pp. 186–195.

5 Choi, S., Enhancing thermal conductivity of fluids with nanoparticles, in: D.A. Siginer, H.P.

6 Masuda, H., Ebata, A,Teramae, K., Hishinuma, N., (1993), Alteration of thermal conductivity and viscosity of liquid by dispersing ultra-fine particles, NetsuBussei (Japan), Vol.7, No.4, pp.227–233.

7 Eldabe, N. T., Elbashbeshy, E. M. A., Elsaid, E. M.,(2013), Effects of Magnetic Field and Heat Generation on Viscous Flow and Heat Transfer over a Nonlinearly Stretching Surface in a Nanofluid, International Journal of Applied Mathematics, ISSN:2051-5227, Vol.28, Issue.1

8 Erigen, A. C., (1966), Theory of micropolar fluids, J. math. Mech., Vol. 16, pp.1-18.

9 Arpaci, V.S., (1968), Effects of thermal radiation on the laminar free convection from a heated vertical plate, Int. J. Heat Mass Transfer, Vol.11, pp.871-881.

10 Cess, R.D., (1966), Interaction of thermal radiation with free convection heat transfer, Int. J. Heat Mass transfer, Vol.9, pp.1269-1277.

11 Cheng, E.H and Ozisik, M.N., (1972), Radiation with free convection in an absorbing emitting and scattering medium, Int. J. Heat Mass Transfer, Vol.15, pp.1243-1252.

12 Raptis, A., (1998), Radiation and free convection flow through a porous medium, Int. Comm. Heat Mass Transfer, Vol.25(2), pp.289-295.

13 Hossain, M.A. and Takhar, H.S., (1996), Radiation effects on mixed convection along a vertical plate with uniform surface temperature, Heat Mass Transfer, Vol.31, pp.243-248.

14 Hossain, M.A. and Takhar, H.S., (1999), Thermal radiation effects on the natural convection flow over an isothermal horizontal plate, Heat Mass Transfer, Vol.35, pp.321-326.

15 Oahimire, J. I., Olajuwon, B.I., Waheed, M. A., and Abiala, I. O., (2013), Analytical solution to mhd micropolar fluid flow past a vertical plate in a slip- flow regime in the presence of thermal diffusion and thermal radiation, Journal of the Nigerian Mathematical Society, Vol. 32, pp. 33-60.

16 El-Arabawy, H.A.M., (2003), Effect of suction/injection on the flow of a micropolar fluid past a continuously moving plate in the presence of radiation, *Int. J. Heat Mass Transfer*, Vol.46, pp. 1471–1477.

17 Ogulu, A., (2005), On the oscillating plate-temperature flow of a polar fluid past a vertical porous plate in the presence of couple stresses and radiation, *Int. comm. Heat Mass Transfer*, Vol.32, pp. 1231–1243.

18 Rahman, M. M. and Sattar, M. A., (2006), Magneto hydrodynamic convective flow of a micropolar fluid past a continuously moving vertical porous plate in the presence of heat generation/absorption, *ASME J. H. Transfer*, Vol.128, pp. 142–152.

19 Nor Azian Aini Mat, Norihan M Arifin, Roslinda Nazar and Fudziah Ismail, (2012), Radiation effect on Marangoni convection boundary layer flow of a nanofluid, Mathematical Sciences, 6:21.

20 Sparrow, E.M. and Cess, R.D., (1961), Temperature-dependent heat sources or sinks in a stagnation point flow, Applied Scientific Research, Vol.A10, pp.185-189.

21 Pop, I. and Soundalgekar, V.M., (1962), Viscous dissipation effects on unsteady free convection flow past an infinite plate with constant suction and heat source, Int. J. Heat Mass Transfer, Vol.17, pp.85-92.

22 Rahman, M. M. and Sattar, M. A., (2007), Transient convective flow of micropolar fluid past a continuously moving vertical porous plate in the presence of radiation, *Int. J. App. Mech. Engi.*, Vol.12(2), pp. 497–51.

23 Yanhai Lin, Liancun Zheng and Xinxin Zhang, (2012), Marangoni Convection Flow and Heat Transfer in Pseudoplastic Non-Newtonian Nanofluids with Radiation Effectsand Heat Generation or Absorption Effects, numerical analysis and applied mathematics, AIP Con.Proc., 1479, pp.50-53.

24 Chamkha, A.J., (2000), Thermal radiation and buoyancy effects on hydromagnetic flow over an accelerating permeable surface with heat source or sink, Int.J.Heat Mass Transfer, Vol.38, pp.1699-1712.

25 Jain, M.K., Iyengar, S.R.K. and Jain, R.K., (1985), Numerical Methods for Scientific and Engineering Computation, Wiley Eastern Ltd., New Delhi, India.